IEEE Access
Multidisciplinary ⋮ Rapid Review ⋮ Open Access Journal

Received 24 December 2023, accepted 6 January 2024, date of publication 9 January 2024,
date of current version 18 January 2024.

Digital Object Identifier 10.1109/ACCESS.2024.3351759

RESEARCH ARTICLE

Microstructure and Microhardness of Conical-Shaped W-Cu Composites Prepared by Spark Plasma Sintering and Subsequent Spinning Process

NGUYEN MINH TUAN[1,2,3], NGUYEN VAN TOAN[1], LUONG VAN DUONG[1], VU THANG LONG[3], TRAN BAO TRUNG[1], PHAM VAN TRINH[1,2], AND DOAN DINH PHUONG[1]

[1]Institute of Materials Science, Vietnam Academy of Science and Technology, Hanoi 10072, Vietnam
[2]Graduate University of Science and Technology, Vietnam Academy of Science and Technology, Hanoi 10072, Vietnam
[3]Institute of Technology, Hanoi 11909, Vietnam

Corresponding author: Doan Dinh Phuong (phuongdd@ims.vast.ac.vn)

ABSTRACT In this study, we present some results on the preparation of a conical-shaped W-Cu composite by using the combination of the spark plasma sintering and subsequent spinning process. The experimental results demonstrated that the full density, fine grain and high hardness composite could be obtained. The relative density of the W-Cu composite after the spinning process increased up to 99.8% which is higher than that of the composite prepared by SPS processing (98.8%). Similarly, the microhardness of the composite after the spinning process is improved compared to the sample obtained after SPS processing. This was attributed to the grain size refinement and the increase of the dislocation density generated during the spinning process. Besides, the dependence of the microstructure and microhardness of the conical-shaped W-Cu composite on the positions of the cone was investigated in detail. As a result, the microstructure and microhardness of the cone were altered at various locations from the inside to the outside walls. This could be attributed to the difference in the interface bond strength between W and Cu matrix at different positions. The current work promises to be an innovative and encouraging approach to producing high-performance W-Cu composites for possible industrial applications and specially in shaped charge liners.

INDEX TERMS W-Cu composite, microstructure, microhardness, spark plasma sintering, spinning.

I. INTRODUCTION

Because of their superior mechanical properties, good wear resistance, low thermal expansion, and high thermal conductivity, W-Cu composites have recently become very important in the automotive, electrical, and military industries [1], [2], [3], [4]. The requirement for the improvement of their mechanical properties is important in order to make them more durable, more reliable, and lower repair costs [1]. So far, many studies have suggested that improving the microstructure of W-Cu composites is a good way to improve their performance [4], [5], [6], [7]. Also, it is well-known that when the grain size reduces to the nanoscale, the characteristics like hardness, tensile ductility, and wear resistance will be improved significantly [8]. However, due to the significant differences in melting points, densities, and mutual solubility, W-Cu composites with ultra-fine grain are extremely challenging to fabricate [9], [10]. Powder metallurgy (PM) technology is often used for fabricating W-Cu composites [1], [2]. It is required to have a high sintering temperature and a long holding time in order to achieve the required level of densification when fabricating pseudo-alloys such as

The associate editor coordinating the review of this manuscript and approving it for publication was Agustin Leobardo Herrera-May.

W-Cu [9], [11], [12]. However, grain coarsening is unavoidable, and copper may leach out of the skeleton, which causes copper segregation, which in turn causes a non-homogenous microstructure and poor product performance. The most common approach used in the fabrication of W-Cu composites is known as melt infiltration [13], [14], [15]. Specifically, W-Cu composites with high tungsten concentrations (>80%) can be only prepared using the melt infiltration process. However, this technique remains some defects such as pores, copper lakes, and tungsten agglomerates, resulting in a low-quality product [16], [17]. Some other techniques such as microwave sintering, hot extrusion, metal powder injection molding, mechanical alloying and liquid sintering have been also used to fabricate W-Cu composites [18], [19], [20], [21], [22], [23], [24]. However, these techniques still require a high sintering temperature and a long holding time. Recently, a promising processing technology known as spark plasma sintering (SPS) has undergone widely used in the fabrication of Cu-W composites [25], [26], [27], [28], [29]. Several studies have demonstrated that the SPS technique can rapidly consolidate powders to a high relative density sample at a low sintering temperature compared to conventional sintering techniques. In addition, SPS also allows the preparation of the samples with finer and more uniform grain and thus resulting in the improvement in the mechanical properties. However, most of the study on W-Cu composites fabricated via the SPS method is focused on how the copper content and sintering conditions (i.e., temperature and pressure, etc.) affect the microstructure and performance of W-Cu composites [9], [25], [28]. It is noted that the samples with cylinder shapes were usually prepared by SPS for further characterization. However, it is well-known that W-Cu composites could be used in some of the applications and specially in liners of some specialty shaped charges. A dense, ductile metal is needed to achieve the deepest penetrations. The most common shape of the liner is conical, with an internal apex angle of 40^{o} to 90^{o}. To our best knowledge, there is no study working on using the SPS technique to prepare W-Cu composite with conical shape for the microstructure and performance analysis up to now.

Additionally, some metal forming techniques such as spinning, rolling, drawing, forging, and bending have been also used for proceeding and deforming in order to obtain the metal alloys or their composites with finer and uniform grains [30], [31]. Among these techniques, an advanced continuous and local metal forming technology called spinning which involves gradually shaping a rotating blank over a mandrel to create rotationally symmetrical structures [32], [33], [34]. Complex pieces with an interior rib or groove can be produced using the spinning technique. One of the essential components, the conical parts with transverse inner rib has been extensively employed in a variety of industries, such as aerospace, astronautics, the military, and other sectors [34]. According to above comments, the combination between SPS technique and spinning technology could be a promising approach to preparing W-Cu composites with full density, fine and uniform grains and thus obtaining high-performance composites for potential applications. The impact of the approach on the structure and performance characteristics of W-Cu composites has not been explored so far. In order to provide ways to optimize the processing approach, it is required to evaluate the effect of the SPS processing and spinning technique on the properties of W-Cu composites.

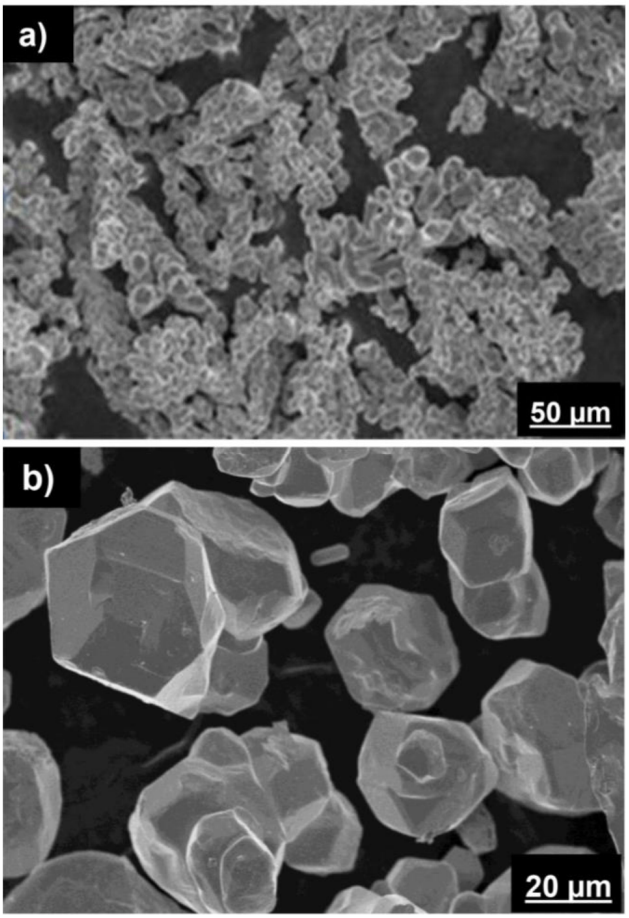

FIGURE 1. SEM image of (a) Cu powder and (b) W powder.

Thus, this study aims to prepare the full density, fine grain and high performance of W-Cu composite with a conical shape for the first time using the combination of the SPS processing and the spinning technique. The microstructure and microhardness of the composites at different positions were investigated and presented.

II. EXPERIMENTAL

A. MATERIALS

A commercial Cu powder (purity of 99.5%) with a particle size in the range of 44-74 μm was supplied by Xilong Chemical Co Ltd., China (**Fig 1a**). The W powder with a purity of 99.9%, angular shape, and the particle size in the range of 20-70 μm was supplied by TaeguTec Co Ltd, Korea (**Fig 1b**).

B. FABRICATION OF W-Cu COMPOSITE

The fabrication process of the W-Cu composite by spark plasma sintering and the subsequent spinning process is

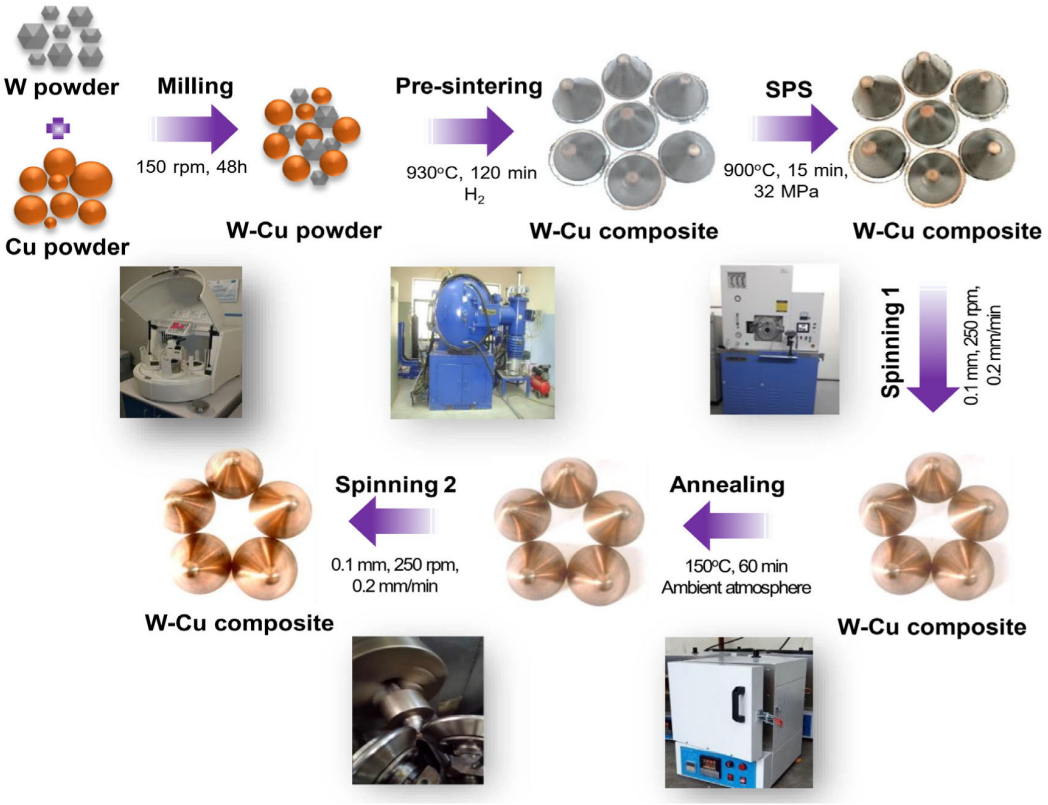

FIGURE 2. The schematic view of the fabrication process of the W-Cu composite by spark plasma sintering and subsequent spinning process.

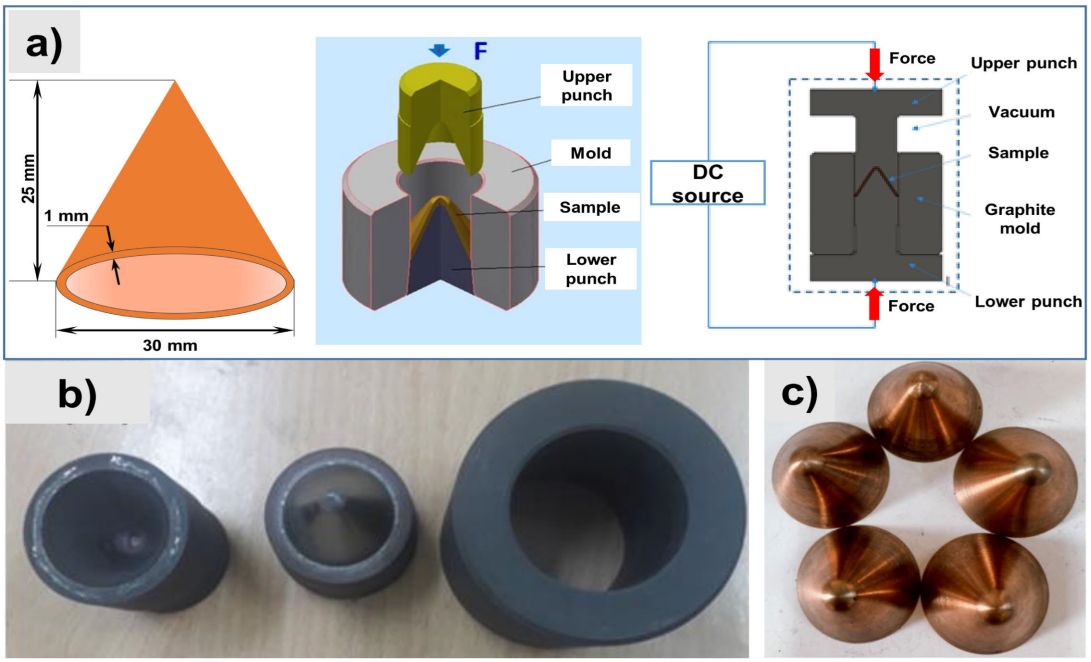

FIGURE 3. (a) The detail of shape and size, (b) graphite molds and (c) optical image of the fabricated conical-shaped W-Cu composite.

described in **Fig 2**. First, W and Cu powders with 1:1 weight ratio along with 1% paraffin added as a binder and 10% n-hexane medium were mixed with a speed of 150 rpm for 48h to obtained uniform dispersed powder using a W-Co hard alloy balls, the ratio of balls to powder is 2/1. After mixing, the powder is taken out and dried in a vacuum oven at

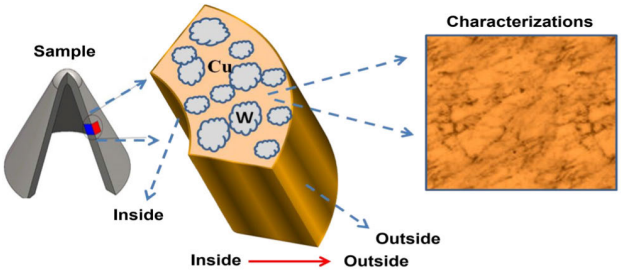

FIGURE 4. Sampling location to observe the microstructure of prepared samples.

60°C for 24h under a pressure of 200 mbar. Next, the Cu-W powder mixture after drying was pressed in a conical mold (**Fig 3**) under a pressing pressure of 6 MPa. After pressing and shaping, the billet is put into a pre-sintering process conducted at a temperature of 930°C for 120 minutes under a hydrogen atmosphere to obtain the necessary strength before being sent to the sintering stage by the SPS technique. After the pre-sintering process, the samples were cleaned and put into a graphite mold for SPS processing using SPS Labox 350 system (Sinterland, Japan) with pulsed DC current (5 μs ON, 5 μs OFF and without any pause). The SPS process was carried out at a temperature of 900°C for 15 minutes under a pressing pressure of 32 MPa in a vacuum (6 Pa). The heating and cooling rates during SPS were 50°C/min. After the SPS process, the sintered samples were further proceeded by two stages of the spinning process to obtain full density and fine grain composites. In spinning 1, the samples were treated three times by the spinning process with the parameters of the spindle speed being 250 rpm, the feed rate of the roller being 0.2 mm/min and the press amount of 0.1 mm. After spinning 1, the samples were annealed to relieve stress at a temperature of 150°C for 60 minutes at ambient atmosphere with the heating and cooling rate of 5°C/min. Next, the samples were introduced in the spinning 2, with the parameters of the spindle speed is 250 rpm, the feed rate of the roller being 0.2 mm/revolution and the press amount of 0.1 mm. The process was repeated two times.

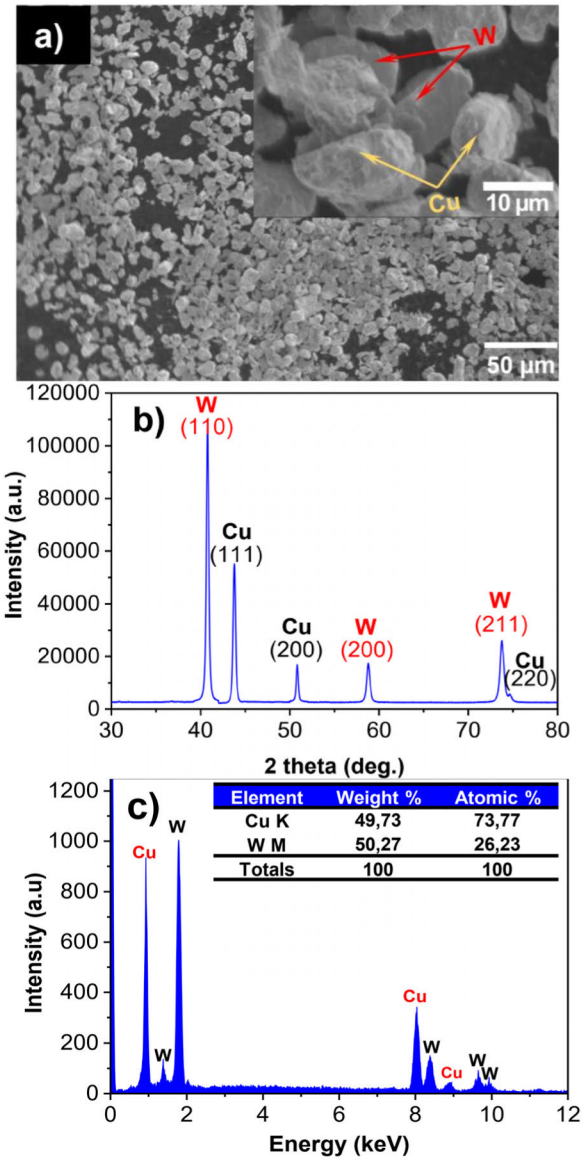

FIGURE 5. (a) SEM image, (b) XRD pattern and (c) EDS spectrum and the elemental content of the milled W-Cu composite powder.

C. CHARACTERIZATION

To study the structure of the conical-shaped W-Cu composite, the sample was taken from the center position by using the wire cutting method as shown in **Fig 4**. Then the sample was ground, polished and etched with an etchant solution of $FeCl_3$ solution (5g) + HCl (10mL) + H_2O (100mL). The microstructure of the samples was studied using optical microscopy (Axiovert 40 MAT, Germany), scanning electron microscopy (SEM, Hitachi S4800, Japan) and transmission electron microscopy (TEM, JEOL JEM 2100, Japan).

The density of the sample was determined by using the Archimedes method (AND GR-202, Japan) in distilled water at room temperature. The reported values are an average of five measurements taken for each examined sample. The relative density of the samples was evaluated by comparing theoretical and experimental density. The theoretical density of W-Cu (1:1) composite was calculated to be 12.23 g/cm^3. The XRD patterns of the samples were recorded in a range of 20°–80° by using X-ray diffraction (XRD, Bruker D8 advance, Germany) with radiation of Cu Kα ($\lambda = 1.5406$ Å) operating at 40 kV and 40 mA, scan step 0.03° and scan rate 0.01 s/step. The XRD patterns were analyzed using MDI Jade 6.0 software. The microhardness of the samples was measured on a microhardness tester (IndentaMet 1106, Buehler USA). To evaluate the accurate hardness measurement results, the samples were made with five measurements at different positions with a load of 0.2 kgf and a holding time of 10 seconds. The reported microhardness value is the average value of ten samples.

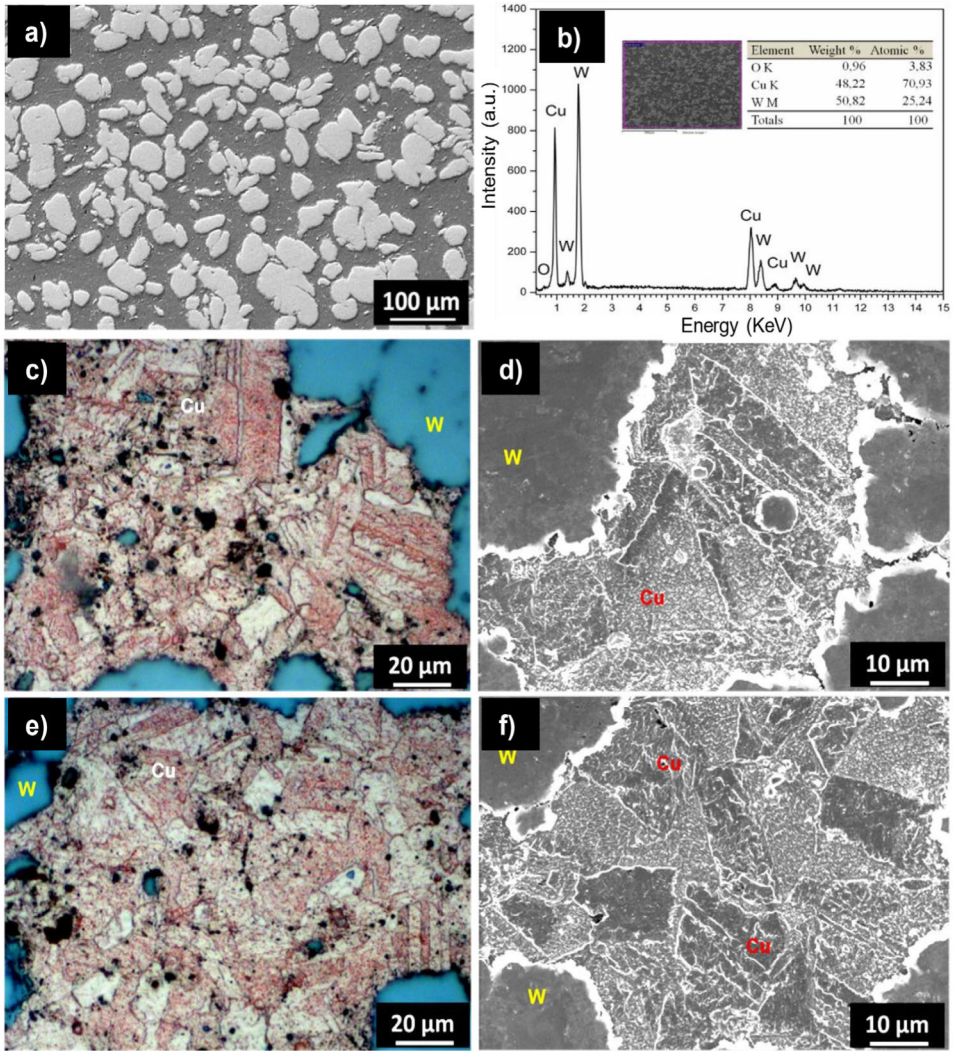

FIGURE 6. (a) SEM image and (b) EDS spectrum of W-Cu composite after SPS processing, optical and SEM image of the cone after etching (c-d) outside and (e-f) inside.

III. RESULTS AND DISCUSSION

A. MICROSTRUCTURAL ANALYSIS

Microstructure of W-Cu composite powder after milling is shown in **Fig 5a**. As can be seen, Cu and W powders were mixed and uniform dispersed together. The XRD pattern of the W-Cu composite powder are shown in **Fig 5b**. The obtained data indicated that only the typical Cu and W peaks could be found. The typical peaks of Cu are located at 2θ of 43.8°, 50.9° and 74.4° which correspond to (111), (200) and (220) planes, respectively (JCPDS No. 003–1018). Meanwhile, the typical peaks of W are determined at 2θ of 40.3°, 58.2° and 73.2° corresponding to (110), (200) and (211) planes, respectively (JCPDS No. 04–0806). This suggested that the phase composition of the W-Cu composite powder is unaffected by the milling process. EDS spectra were used to examine the chemical compositions of the W-Cu composite powder. As shown in **Fig 5c**, the powder consist of two primary components of the composite are Cu and W with the content of 49.73% and 50.27 wt.%, respectively. This is in a good agreement with the designed samples.

Fig 6a is the SEM image of the conical-shaped W-Cu composite after SPS processing. As can be seen, it shows quite uniform dispersion of W particles (white) on Cu background (gray). The chemical compositions of the W-Cu composite were analyzed by EDS spectra as shown in **Fig 6b**. It showed that the composite consists of two main components including Cu and W with an amount of 48.22 wt.% and 50.82%, respectively. There is a slight difference between the Cu and W contents as designed. In addition, a small amount of oxygen with content $<$ 1 wt.% can also be analyzed. This is possible due to the possible amount of oxygen on the surface of Cu and W particles during the sample fabrication. However, with a low oxygen content of less than 1 wt.%, it can also be considered as a sintering process that does not cause oxidation for conical-shaped Cu-W composite. SEM images and optical images of Cu-W composite after SPS

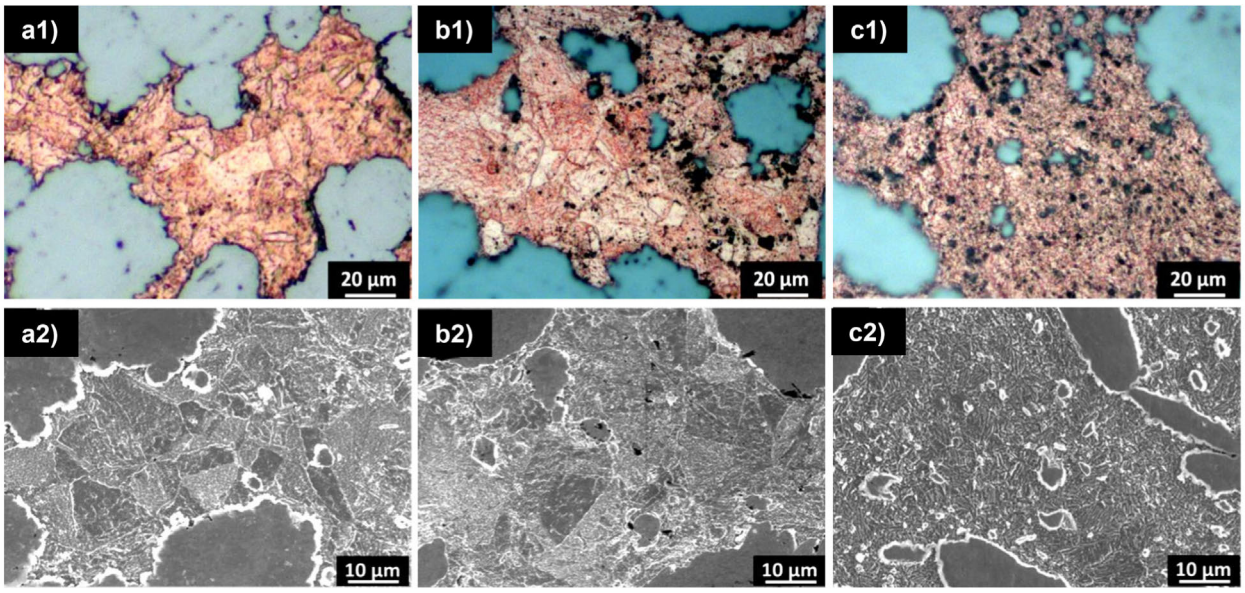

FIGURE 7. Optical images and SEM images of W-Cu composite samples processed by SPS and spinning 1 at different position (a1-a2) inside, (b1-b2) center and (c1-c2) outside.

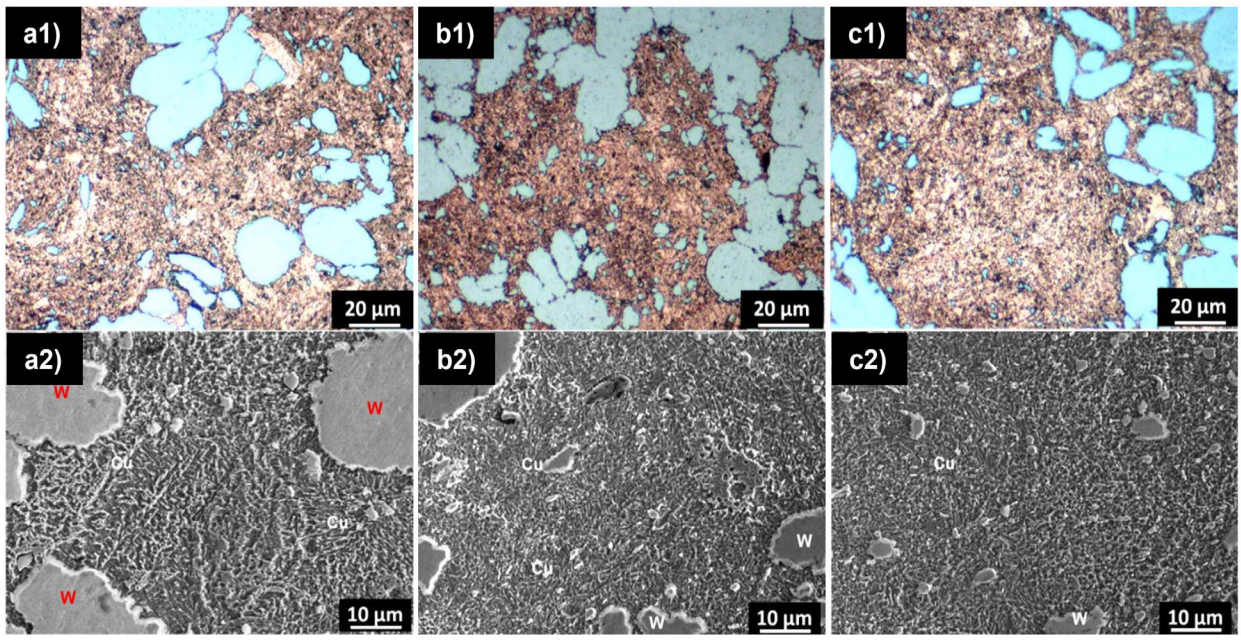

FIGURE 8. Optical images and SEM images of W-Cu composite processed by SPS, spinning 1, annealing, and spinning 2 at different position (a1-a2) inside, (b1-b2) center and (c1-c2) outside.

processing are shown in **Fig 6**, where mainly the structure of the Cu-rich region is observed. **Fig 6c-d** corresponds to the optical image and SEM image of the area near the outside surface of the cone. **Fig 6e-f** is an optical image of the area near the inside surface of the cone. The structure of the Cu matrix contains many grains with a size distribution from a few tens of micrometers to hundreds of nanometers. Thus, the structure going from the outside to the inside of the cone is nearly the same, there is not much difference in particle shape and size.

The cones after SPS processing were annealed at 150°C for 60 minutes to relieve stress, then proceed to the first spinning process. The sample after the spinning 1 is also cut at the same positions as the sample for the cone as shown in Fig. 4 and marked on the inside and outside of the cone wall for convenience in the observation and evaluation process.

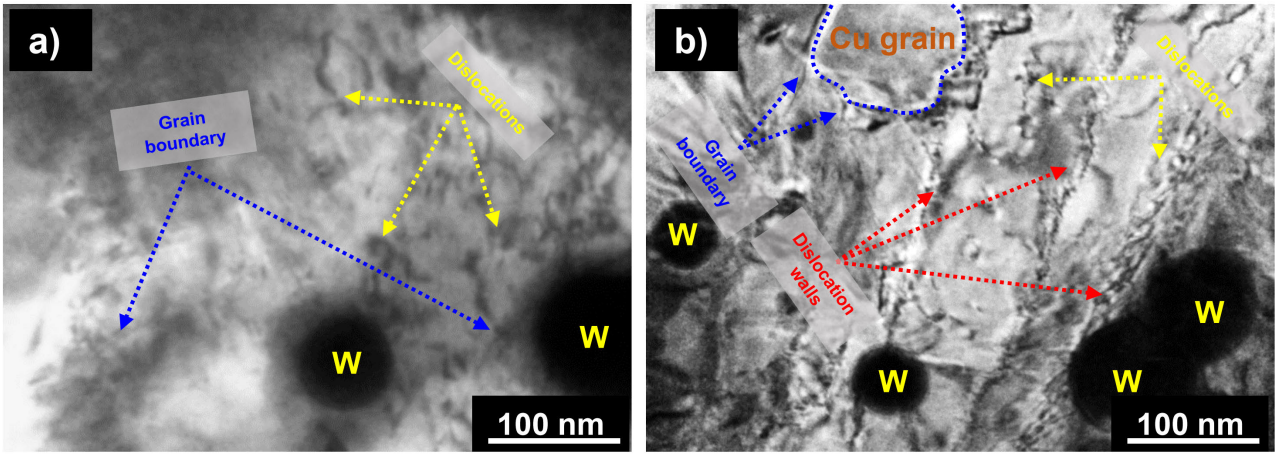

FIGURE 9. TEM images of W-Cu composite processed by (a) SPS and spinning 1 and (b) SPS, spinning 1, annealing and spinning 2.

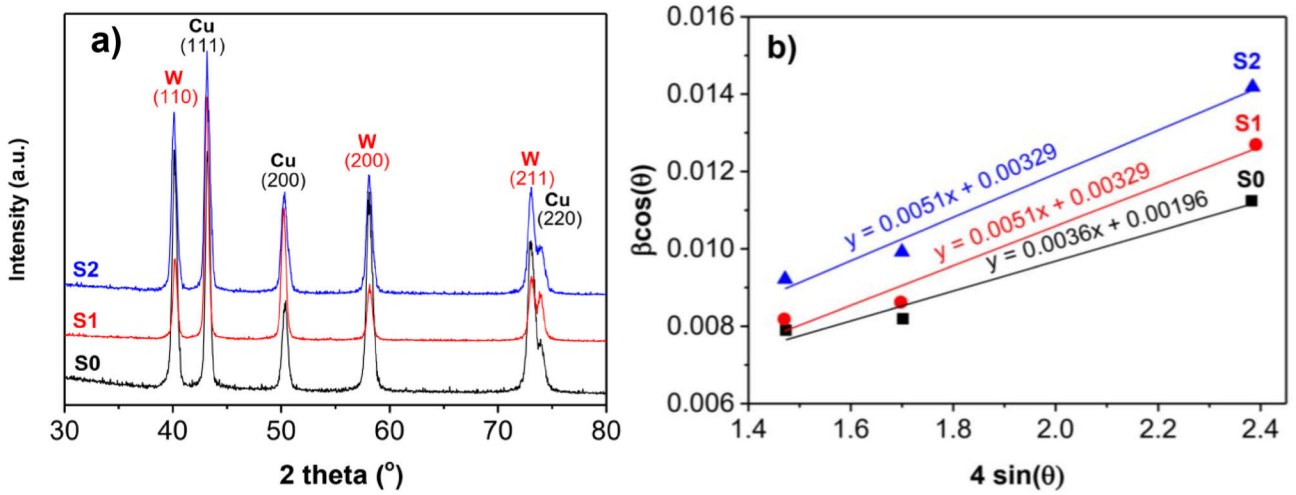

FIGURE 10. (a) XRD patterns of W-Cu composite processed by (S0) SPS processing, (S1) SPS and spinning 1, (S2) SPS, spinning 1, annealing and spinning 2 and (b) plotting and linearly fitting the relationship between $\beta\cos\theta$ and $4\sin\theta$.

Fig 7a1, 7b1 and **7c1** are optical images of the cone section after spinning, polishing and etching at positions corresponding to the structure of the section going from the inside surface to the outside surface of the cone. It can be seen in the inside surface of the cone wall (**Fig 7a1**), the Cu-rich area has a structure similar to that of the cone wall after SPS processing, that is, in copper grains containing many particles with rather large sizes up to few tens of micrometers. In the center of the cone wall, the structure shows that there are still many Cu particles with large sizes, but some areas have changed into smaller particles and the grain boundaries are not observed (**Fig 7b1**). Coming to the outside region, the microstructure of the copper-rich area is not clearly defined the grain boundary between the copper grains. This could be because of the copper particles became finer during the deformation process (**Fig 7c1**). To see more clearly the structure of the cone wall after spinning 1, the cross-sectional structure was further observed through SEM as shown in **Fig 7a2, 7b2** and **7c2.** The corresponding imaging areas from the inside surface to the outside of the cone walls are taken in the same as for optical images. Observational results also clearly show that, for the area on the inside and the center of the cone wall, the Cu grains are larger. However, the Cu grains were deformed and become smaller in the area of the outside cone surface. When observed at higher magnification, for the area outside the cone surface, the microstructure of the copper-rich region consists of small grains with a size of a few hundred nanometers. This demonstrated that the spinning process is possible to form the ultra-fine grain structure on the outside surface of the cone. However, the inside surface of the cone still retains the coarse-grained structure similar to after SPS processing. The grain size transformation produces a grain size gradient from the inside to the outside of the conical-shaped W-Cu composite with a relation of the coarse grain to an ultra-fine-grained structure.

Fig 8 shows the cross-sectional optical image and SEM image of the cone with the corresponding positions from the inside to the outside of the cone wall of the sample after the spinning 2. Observation of the optical image, there is no longer appearance of coarse Cu grain from the inside to the outside wall of the cone. This result demonstrated that after spinning 2, the grain structure of copper in the entire cone wall has been affected by the spinning process and creates an ultra-fine-grained structure. This is further clarified through SEM observations as shown in **Fig 8a2, 8b2** and **8c2**. As can be seen, the Cu-rich regions completely contain mainly ultra-fine grains with a bar-like structure or stacked plates with sizes ranging from a few μm to hundreds of nm. Thus, after two spinning processes, the Cu-rich regions is completely transformed into an ultra-fine structure.

To clarify the influence of the spinning process, the outside surface structure of the cone was observed on transmission electron microscopy. **Fig 9a** is the TEM image of the conical-shaped W-Cu composite after spinning 1. As observed on the TEM image, it clearly shows ultra-fine grains with a size of several hundred nm. Furthermore, from the TEM images, many dislocations are also observed in the Cu grains. Besides, the dislocations tend to aggregate together to form dislocation walls at the grain boundary positions. The appearance of the dislocations is due to the continuous deformation of large grains to form small grains during the spinning process. When this deformation process becomes strong, the dislocations also gradually move to the grain boundary regions to form the dislocation walls. The structure of Cu matrix after spinning 2 is also observed on the TEM image to evaluate the change compared with the composite prepared after spinning 1 (**Fig 9b**). As can be seen, it is clear that the formation of the dislocations in the ultra-fine grains is observed. In addition, the stronger and more concentrated formation of dislocation walls is also observed at the grain boundary positions compared with the structure of the composite after the spinning 1.

Xray diffraction was used to validate the transmission electron microscopy study. **Fig 10a** shows XRD patterns of the W-Cu composite after SPS processing (S0), after the spinning 1 (S1) and after the spinning 2 (S2). From the XRD patterns, it is shown that the sample consist only of Cu and W with typical peaks as noted in **Fig 10a**. This confirm that the sintering and spinning process do not change the phase composition of the composite. Using the Xray diffraction data, the dislocation density (ρ) in all samples was calculated by using the following Equation (1) [35]:

$$\rho = \frac{2\sqrt{3}\varepsilon}{d_c b} \tag{1}$$

where b is the dislocation Burgers vector, and using the Williamson-Hall method described in Equation (2) [36], it is possible to determine the microstrain (ε) and crystalline size (d_c) of the samples from the XRD peak broadening (β_{hkl}):

$$\beta_{hkl}\cos\theta = \frac{0.94\lambda}{d_c} + 4\varepsilon\sin\theta \tag{2}$$

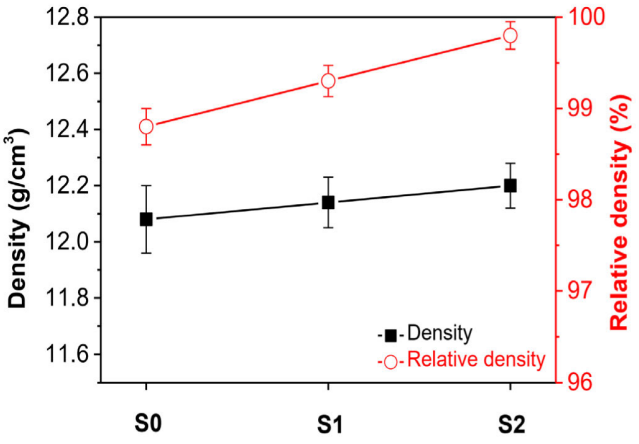

FIGURE 11. Density and relative density of W-Cu composite processed by (S0) SPS processing(S1) SPS and spinning 1, (S2) SPS, spinning 1, annealing and spinning 2.

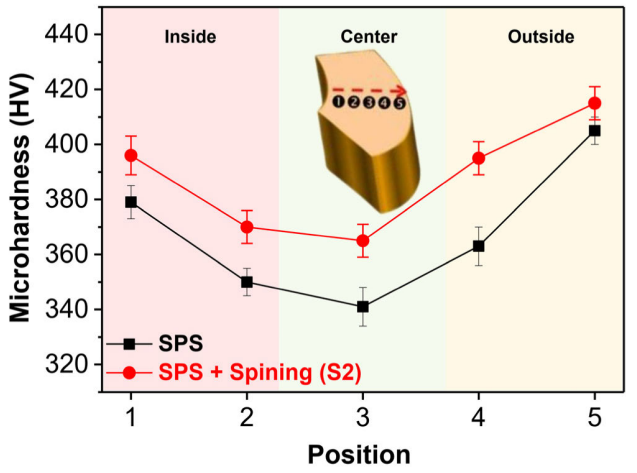

FIGURE 12. Microhardness of W-Cu composite processed by (S0) SPS processing and (S2) SPS processing and spinning 2.

where λ is the wavelength of Cu K_α radiation. By plotting and linearly fitting the relationship between $\beta\cos\theta$ and $4\sin\theta$ (**Fig 10b**), the values of ε and dc were estimated using the slope and intercept. The d_c of the composite was calculated to be 70.7 nm, 41.2 nm and 20.1 nm corresponding to the W-Cu composite (S0) after SPS processing, (S1) after SPS processing and spinning 1 and (S2) after SPS processing and spinning 2, respectively. The obtained results are in good agreement with the measured results observed by the microstructural analysis as discussed in the above section. Besides, the value of dislocation density (ρ) was calculated using Equation (2) to be 7.38×10^{14} m^{-2}, 1.65×10^{15} m^{-2} and 3.78×10^{15} m^{-2} for the S0, S1 and S2, respectively. As a result, the dislocation density of the W-Cu composite was increased with the number of the spinning process. Thus, the spinning process not only reduces the grain size but also increase the dislocation density of the composite. This will be a key factor that leads to the improvement in the mechanical properties of the W-Cu composites.

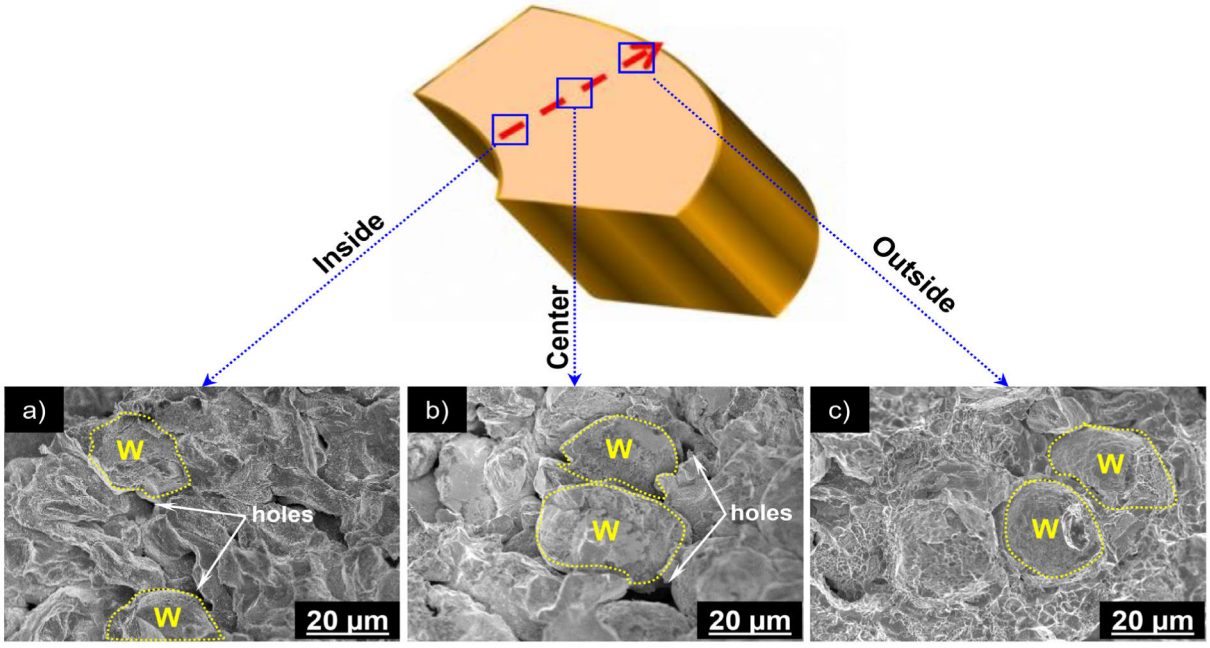

FIGURE 13. Fracture surfaces of conical shaped W-Cu composite at different regions (a) inside, (b) center and (c) outside.

B. DENSITY AND MICROHARDNESS

In addition to the microstructure, the spinning process also increases the density of the conical-shaped W-Cu composite. The density and relative density of the W-Cu composite were presented in **Fig 11**. After SPS processing, the density of the W-Cu composite cone was measured to be 12.08 ± 0.12 g/cm^3, corresponding to the relative density of 98.8 ± 0.2%. After the first and second spinning processes, the density of the composite increased to 12.14 ± 0.09 g/cm^3 and 12.2 g/cm^3 ± 0.08 g/cm^3, respectively, corresponding to the relative density of 99.3 ± 0.17% and 99.8 ± 0.15%, respectively. The increase in the density could be due to the pores that may exist in the cone structure having been removed by the spinning process.

To evaluate the effect of the spinning process on the hardness of the conical-shaped W-Cu composite, samples were also cut from the conical wall and ground, polished, and then measured with a Vickers microhardness tester at different positions from the inside to outside walls of the cone. **Fig 12** shows the microhardness of the composite after SPS processing (S0) and after SPS processing and spinning 2 (S2). As can be seen, the general trend is the hardness on the outside wall of the composites remains a higher microhardness than that of the inside wall. For composite after SPS processing the highest hardness is obtained at the outside wall positions of the cone with a value of 379 ± 6 HV followed by the microhardness of positions located at the inside wall of the cone. The lowest microhardness was measured at the position located at the center of the cone with a value of 341 ± 7 HV. For cones after SPS processing and then proceeding with the spinning process, the highest microhardness was measured to be 415 ± 6 HV, 396 ± 8 HV and 365 ± 5 HV corresponding to the positions at the outside wall, the inside wall and the center of the cone. It is noted that the microhardness of the composite after the spinning process was higher compared to the sample obtained after SPS processing. This could be resulted from the increase in the dislocation density generated during the spinning process as demonstrated by TEM and XRD analysis. Besides, the improvement in the microhardness could be attributed to the decrease in the Cu grain size according to the Hall–Petch relation as given by Equation (3) [37], [38]:

$$H_C = H_{C0} + kd_c^{-1/2} \tag{3}$$

where H_C is the microhardness of the conical-shaped W-Cu composite, k is the Hall–Petch coefficient, and dc is the Cu grain size. According to **Equation (3)**, the decrease in the grain size is a key factor leading to enhancing the microhardness of the composites. In this study, the Cu grain size of the composite decreased significantly from coarse to ultra-fine grain after the spinning process as discussed in the above section. In addition, it is interestingly noted that the microhardness of the conical-shaped W-Cu composites is different as measured at different positions from the inside wall to the outside wall of the cone. This could be due to the difference in the interface bond strength between W and Cu matrix at different positions. **Fig 13** shows the fracture surfaces of the composites at different positions from the inside to outside walls of the cone. As can be seen, the interface bond strength between W and Cu matrix at the outside region is much stronger than that of other regions. In which, there are no gaps between W and Cu that can be observed. On the contrary, some holes and gaps between W and Cu were observed at the inside and center regions of cone. This

implied that the interface bond strength between W and Cu at these regions is weaker compared to that of the outside region. The decrease in the W-Cu bond strength led to the reduction in the load transfer strengthening from the softer and weaker Cu matrix to harder W reinforcement and thus resulting in the decrease in microhardness of the composites at the inside and center regions of the cone.

IV. CONCLUSION

We have successfully prepared the full density, fine grain and high hardness conical-shaped W-Cu composite by using the combination of the spark plasma sintering and subsequent spinning process. After the spinning process, the relative density of the W-Cu composite increased to 99.8%, exceeding the relative density of the composite made via SPS processing (98.8%). The microhardness of the composite following the spinning process is higher than the sample produced throughout SPS processing. In addition, the microstructure and microhardness of the conical-shaped W-Cu composite at different positions were investigated. The obtained results demonstrated that the microhardness of the prepared composites varies from the inner wall to the outer wall of the cone. The proposed study has the potential to be an innovative and encouraging new method for developing high-performance W-Cu composites for use in future industrial applications.

REFERENCES

[1] L. L. Dong, M. Ahangarkani, W. G. Chen, and Y. S. Zhang, "Recent progress in development of tungsten-copper composites: Fabrication, modification and applications," *Int. J. Refractory Met. Hard Mater.*, vol. 75, pp. 30–42, Sep. 2018, doi: 10.1016/J.IJRMHM.2018.03.014.

[2] C. Hou, X. Song, F. Tang, Y. Li, L. Cao, J. Wang, and Z. Nie, "W–Cu composites with submicron- and nanostructures: Progress and challenges," *NPG Asia Mater.*, vol. 11, no. 1, pp. 1–20, Dec. 2019, doi: 10.1038/s41427-019-0179-x.

[3] T. Bregel, W. Krauss-Vogt, R. Michal, and K. E. Saeger, "On the application of W/Cu materials in the fields of power engineering and plasma technology," *IEEE Trans. Compon., Hybrids, Manuf. Technol.*, vol. 14, no. 1, pp. 8–13, Mar. 1991, doi: 10.1109/33.76502.

[4] T. Han, C. Hou, Z. Zhao, X. Huang, F. Tang, Y. Li, and X. Song, "W–Cu composites with excellent comprehensive properties," *Composites Part B: Eng.*, vol. 233, Mar. 2022, Art. no. 109664, doi: 10.1016/J.COMPOSITESB.2022.109664.

[5] H. Ibrahim, A. Aziz, and A. Rahmat, "Enhanced liquid-phase sintering of W–Cu composites by liquid infiltration," *Int. J. Refractory Met. Hard Mater.*, vol. 43, pp. 222–226, Mar. 2014, doi: 10.1016/J.IJRMHM.2013.12.004.

[6] M. Ahangarkani and K. Zangeneh-madar, "Investigation on the microstructure and properties of W-10 wt% Cu prepared by sintering and infiltration," *Int. J. Refractory Met. Hard Mater.*, vol. 75, pp. 1–9, Sep. 2018, doi: 10.1016/J.IJRMHM.2018.03.015.

[7] L. Dong, W. Chen, C. Zheng, and N. Deng, "Microstructure and properties characterization of tungsten–copper composite materials doped with graphene," *J. Alloys Compounds*, vol. 695, pp. 1637–1646, Feb. 2017, doi: 10.1016/J.JALLCOM.2016.10.310.

[8] B. Li, Z. Sun, G. Hou, P. Hu, and F. Yuan, "Fabrication of fine-grained W–Cu composites with high hardness," *J. Alloys Compounds*, vol. 766, pp. 204–214, Oct. 2018, doi: 10.1016/J.JALLCOM.2018.06.338.

[9] X. Li, M. Zhang, G. Zhang, S. Wei, L. Xu, and Y. Zhou, "Effect of spark plasma sintering temperature on structure and performance characteristics of Cu-20 wt%W composite," *J. Alloys Compounds*, vol. 912, Aug. 2022, Art. no. 165246, doi: 10.1016/J.JALLCOM.2022.165246.

[10] A. Mondal, A. Upadhyaya, and D. Agrawal, "Comparative study of densification and microstructural development in W–18Cu composites using microwave and conventional heating," *Mater. Res. Innov.*, vol. 14, no. 5, pp. 355–360, Nov. 2010, doi: 10.1179/143307510X12820854748638.

[11] Q. Zhou and P. Chen, "Fabrication of W–Cu composite by shock consolidation of Cu-coated W powders," *J. Alloys Compounds*, vol. 657, pp. 215–223, Feb. 2016, doi: 10.1016/J.JALLCOM.2015.10.057.

[12] L. Wang, L. Xu, C. Srinivasakannan, S. Koppala, Z. Han, and H. Xia, "Electroless copper plating of tungsten powders and preparation of WCu20 composites by microwave sintering," *J. Alloys Compounds*, vol. 764, pp. 177–185, Oct. 2018, doi: 10.1016/J.JALLCOM.2018.06.061.

[13] L. Dong, W. Chen, L. Hou, N. Deng, and C. Zheng, "W–Cu system: Synthesis, modification, and applications," *Powder Metall. Metal Ceram.*, vol. 56, nos. 3–4, pp. 171–184, Jul. 2017, doi: 10.1007/S11106-017-9884-6.

[14] Y. Guo, J. Yi, S. Luo, C. Zhou, L. Chen, and Y. Peng, "Fabrication of W–Cu composites by microwave infiltration," *J. Alloys Compounds*, vol. 492, nos. 1–2, pp. 75–78, Mar. 2010, doi: 10.1016/J.JALLCOM.2009.12.011.

[15] P. Zhao, S. Guo, G. Liu, Y. Chen, and J. Li, "Fabrication of cu-riched W–Cu composites by combustion synthesis and melt-infiltration in ultrahigh-gravity field," *J. Nucl. Mater.*, vol. 441, nos. 1–3, pp. 343–347, Oct. 2013, doi: 10.1016/J.JNUCMAT.2013.06.011.

[16] S. Mahmoudi and G. Faraji, "Fabrication of functionally graded W Cu composite via variable speed induction sintering and subsequent infiltration," *Int. J. Refractory Met. Hard Mater.*, vol. 106, Aug. 2022, Art. no. 105857, doi: 10.1016/J.IJRMHM.2022.105857.

[17] M. V. Lungu, "Synthesis and processing techniques of tungsten copper composite powders for electrical contact materials a review," *Oriental J. Chem.*, vol. 35, no. 2, pp. 491–515, Apr. 2019, doi: 10.13005/OJC/350201.

[18] M. Roosta, H. Baharvandi, and H. Abdizade, "An experimental investigation on the fabrication of W–Cu composite through hot-press," *Int. J. Ind. Chem.*, vol. 3, no. 1, pp. 1–6, Dec. 2012, doi: 10.1186/2228-5547-3-10.

[19] Y. Li and S. Yu, "Thermal–mechanical process in producing high dispersed tungsten–copper composite powder," *Int. J. Refractory Met. Hard Mater.*, vol. 26, no. 6, pp. 540–548, Nov. 2008, doi: 10.1016/J.IJRMHM.2008.01.001.

[20] P. W. Ho, Q. F. Li, and J. Y. H. Fuh, "Evaluation of W–Cu metal matrix composites produced by powder injection molding and liquid infiltration," *Mater. Sci. Eng., A*, vol. 485, nos. 1–2, pp. 657–663, Jun. 2008, doi: 10.1016/J.MSEA.2007.10.048.

[21] D. Li, Z. Liu, Y. Yu, and E. Wang, "The influence of mechanical milling on the properties of W–40 wt.%Cu composite produced by hot extrusion," *J. Alloys Compounds*, vol. 462, nos. 1–2, pp. 94–98, Aug. 2008, doi: 10.1016/J.JALLCOM.2007.08.042.

[22] M. H. Maneshian and A. Simchi, "Solid state and liquid phase sintering of mechanically activated W–20 wt.% Cu powder mixture," *J. Alloys Compounds*, vol. 463, nos. 1–2, pp. 153–159, Sep. 2008, doi: 10.1016/J.JALLCOM.2007.08.080.

[23] J.-K. Lee, "On the effect of substituting copper powder with cupric salt for the sintering process of W–Cu MIM parts," *Int. J. Refractory Met. Hard Mater.*, vol. 26, no. 4, pp. 290–294, Jul. 2008, doi: 10.1016/J.IJRMHM.2007.06.005.

[24] G. Pintsuk, I. Smid, J. E. Döring, W. Hohenauer, and J. Linke, "Fabrication and characterization of vacuum plasma sprayed W/Cu-composites for extreme thermal conditions," *J. Mater. Sci.*, vol. 42, no. 1, pp. 30–39, Jan. 2007, doi: 10.1007/S10853-006-1039-Y.

[25] A. Elsayed, W. Li, O. A. El Kady, W. M. Daoush, E. A. Olevsky, and R. M. German, "Experimental investigations on the synthesis of W–Cu nanocomposite through spark plasma sintering," *J. Alloys Compounds*, vol. 639, pp. 373–380, Aug. 2015, doi: 10.1016/J.JALLCOM.2015.03.183.

[26] C. Luo, Y. Wang, J. Xu, G. Xu, Z. Yan, J. Li, H. Li, H. Lu, and J. Suo, "The activated sintering of W Cu composites through spark plasma sintering," *Int. J. Refractory Met. Hard Mater.*, vol. 81, pp. 27–35, Jun. 2019, doi: 10.1016/J.IJRMHM.2019.02.015.

[27] L. K. Pillari, S. R. Bakshi, P. Chaudhuri, and B. S. Murty, "Fabrication of W–Cu functionally graded composites using high energy ball milling and spark plasma sintering for plasma facing components," *Adv. Powder Technol.*, vol. 31, no. 8, pp. 3657–3666, Aug. 2020, doi: 10.1016/J.APT.2020.07.015.

[28] S. S. Kalyan Kamal, Y. Sushma, J. Vimala, B. Shankar, P. Ghosal, L. Durai, and B. Majumdar, "Effect of processing route on densification of W-10 wt% Cu nanocomposite using spark plasma sintering," *J. Alloys Compounds*, vol. 785, pp. 1137–1143, May 2019, doi: 10.1016/J.JALLCOM.2019.01.274.

[29] S. Diouf and A. Molinari, "Densification mechanisms in spark plasma sintering: Effect of particle size and pressure," *Powder Technol.*, vol. 221, pp. 220–227, May 2012, doi: 10.1016/J.POWTEC.2012.01.005.

[30] G. Kajal, M. R. Tyagi, and G. Kumar, "A review on the effect of residual stresses in incremental sheet metal forming used in automotive and medical sectors," *Mater. Today, Proc.*, vol. 78, pp. 524–534, Jan. 2023, doi: 10.1016/J.MATPR.2022.11.235.
[31] Z. Ding, H. Wang, J. Luo, and N. Li, "A review on forming technologies of fibre metal laminates," *Int. J. Lightweight Mater. Manuf.*, vol. 4, no. 1, pp. 110–126, Mar. 2021, doi: 10.1016/J.IJLMM.2020.06.006.
[32] Q. Xia, G. Xiao, H. Long, X. Cheng, and X. Sheng, "A review of process advancement of novel metal spinning," *Int. J. Mach. Tools Manuf.*, vol. 85, pp. 100–121, Oct. 2014, doi: 10.1016/J.IJMACHTOOLS.2014.05.005.
[33] F. Ma, H. Yang, and M. Zhan, "Plastic deformation behaviors and their application in power spinning process of conical parts with transverse inner rib," *J. Mater. Process. Technol.*, vol. 210, no. 1, pp. 180–189, Jan. 2010, doi: 10.1016/J.JMATPROTEC.2009.07.006.
[34] O. Music, J. M. Allwood, and K. Kawai, "A review of the mechanics of metal spinning," *J. Mater. Process. Technol.*, vol. 210, no. 1, pp. 3–23, Jan. 2010, doi: 10.1016/J.JMATPROTEC.2009.08.021.
[35] A. Khorsand Zak, W. H. A. Majid, M. E. Abrishami, and R. Yousefi, "X-ray analysis of ZnO nanoparticles by Williamson–Hall and size–strain plot methods," *Solid State Sci.*, vol. 13, no. 1, pp. 251–256, Jan. 2011, doi: 10.1016/J.SOLIDSTATESCIENCES.2010.11.024.
[36] B. Kisan, R. K. Bhuyan, and R. K. Mohapatra, "Nanocrystalline NiO powder: Synthesis, characterization and emerging applications," in *Nano-Biosorbents for Decontamination of Water, Air, and Soil Pollution*. Amsterdam, The Netherlands: Elsevier, Jul. 2022, pp. 529–550, doi: 10.1016/B978-0-323-90912-9.00023-X.
[37] S. N. Naik and S. M. Walley, "The Hall-Petch and inverse Hall-Petch relations and the hardness of nanocrystalline metals," *J. Mater. Sci.*, vol. 55, no. 7, pp. 2661–2681, Mar. 2020, doi: 10.1007/S10853-019-04160-W.
[38] A. S. Taha and F. H. Hammad, "Application of the Hall-Petch relation to microhardness measurements on Al, Cu, Al-MD 105, and Al–Cu alloys," *Phys. Status Solidi (A)*, vol. 119, no. 2, pp. 455–462, Jun. 1990, doi: 10.1002/PSSA.2211190207.

NGUYEN MINH TUAN received the bachelor's degree from the Department of Mechanical of Deformation, Hanoi University of Science and Technology (HUST), Vietnam, in 2001, and the master's degree in machinery manufacturing technology from Le Quy Don Technical University, Hanoi, Vietnam, in 2010. He is currently pursuing the Ph.D. degree in materials science with the Graduated University of Science and Technology (GUST), Vietnam Academy of Science and Technology (VAST), Vietnam. He is also a Researcher with the Institute of Technology. His research interests include composites, superalloys, powder metallurgy, and machinery manufacturing technology.

NGUYEN VAN TOAN received the master's degree from the Hanoi University of Science and Technology, Vietnam, in 2018. He is currently pursuing the Ph.D. degree with the Graduate University of Science and Technology, Vietnam. He is also a Researcher with the Advanced Metallic Materials Department, Institute of Materials Sciences, Vietnam Academy of Science and Technology. His research interests include high entropy alloys and hydrogen storage materials synthesis and characterization.

LUONG VAN DUONG received the bachelor's degree from the Faculty of Materials Science and Technology, Hanoi University of Science and Technology (HUST), Vietnam, in 2006, the master's degree from the Department of Applied Materials Engineering, Chungnam National University, South Korea, in 2012, and the Ph.D. degree in metal science from the Graduated University of Science and Technology, Vietnam, in 2019. He is currently a Senior Researcher with the Department of Advance Metallic Materials, Institute of Materials Science (IMS), Vietnam Academy of Science and Technology (VAST), Vietnam. He has published about 18 articles in peer-reviewed international journals. His research interests include the metal and alloy, hard-coatings, and composite based on metal matrix and ceramics.

VU THANG LONG received the bachelor's and master's degrees in machinery manufacturing technology from Le Quy Don Technical University, Hanoi, Vietnam, in 2012 and 2016, respectively. He is currently a Researcher with the Institute of Technology, Vietnam. His research interests include composites, superalloys, powder metallurgy, and machinery manufacturing technology.

TRAN BAO TRUNG received the bachelor's degree from the Department of Metallurgy, Hanoi University of Science and Technology, Vietnam, in 2004, the master's degree in materials science from the International Institute for Materials Science, Hanoi University of Science and Technology, in 2006, and the Ph.D. degree in materials science from the School of Materials and Mineral Resources Engineering, Universiti Sains Malaysia, Malaysia, 2013. He is currently a Researcher with the Department of Advanced Metallic Materials, Institute of Materials Science, Vietnam Academy of Science and Technology, Vietnam. He has published over ten articles in peer-reviewed international journals. His research interests include metal-ceramic composites, metal porous materials, soft magnetic, and refractory high entropy alloys.

PHAM VAN TRINH received the bachelor's degree and master's degrees in nanomaterials and nanodevices from the Department of Engineering Physics, VNU University of Engineering and Technology, Hanoi, Vietnam, in 2010, and the Ph.D. degree in materials science and engineering from the Graduate University of Science and Technology, Vietnam Academy of Science and Technology, Hanoi, in 2016. He is currently a Principal Researcher with the Institute of Materials Science, Vietnam Academy of Science and Technology. His research interests include carbon nanomaterials, metal matrix composites, hybrid solar cells, and nanofluids.

DOAN DINH PHUONG received the Engineering degree in metallurgy from the Technical University in Košice, Košice, Slovakia, in 1986, and the Ph.D. degree in inorganic materials technology from the Hanoi University of Science and Technology, Vietnam, in 2008. He is currently the Director of the Institute of Materials Science, Vietnam Academy of Science and Technology, Hanoi, Vietnam. His research interests include metal matrix composites, superalloys, and high entropy alloys.